HHS Public Access

Author manuscript

Nat Biomed Eng. Author manuscript; available in PMC 2019 June 06.

Published in final edited form as:

Nat Biomed Eng. 2018 May ; 2(5): 318–325. doi:10.1038/s41551-018-0234-x.

Micelles with Ultralow Critical Micelle Concentration as Carriers for Drug Delivery

Yang Lu, **Zhanguo Yue**, **Jinbing Xie**, **Wei Wang**, **Hui Zhu**, **Ershuai Zhang**, and **Zhiqiang Cao**

Department of Chemical Engineering and Materials Science, Wayne State University, Detroit, MI 48202, USA.

Abstract

Conventional micellar carriers disassemble into free surfactants when diluted at concentrations below the critical micelle concentration (CMC). This limits the bioavailability *in vivo* of injected hydrophobic drugs encapsulated in micellar systems. Here, we show that a micelle comprising a superhydrophilic zwitterionic polymer domain and a superhydrophobic lipid domain has an undetectable CMC below 10^{-6} mM, a value that is orders of magnitude lower than the CMCs ($>10^{-3}$ mM) of typical micellar systems. We also show that zwitterionic moieties or zwitterionic polymers added into a micelle solution stabilize the micelles at concentrations below their inherent CMC. In a mouse model of melanoma, ultralow CMC micelles encapsulating docetaxel led to the complete eradication of tumors, whereas conventional docetaxel micellar formulations did not reverse tumor growth. Ultralow-CMC micelles might become next-generation carriers for drug delivery.

Micelles play a pivotal role in drug delivery.[1–4] They are small sub-50 nm entities physically assembled by water-soluble amphiphilic surfactants and can solubilize hydrophobic drug molecules that are not well dissolved in water. Compared with other drug stabilizing or delivery strategies (ranging from liposomes, polymer or protein-drug conjugates, polymeric nanospheres, to cells or pathogens),[5–22] micelles have been received as the first-line technology.[3] Their molecular structures and assembling behaviors are well defined, and a drug solution stabilized by micelles can be easily manufactured. This enables large scale production and stable clinical performance of the formulations. However, the main challenge with micelles is that all conventional micelles, unless chemically crosslinked,[1–3, 23] will disassemble into free surfactants under diluted conditions (e.g., below critical micelle concentrations, CMC, which is typical when infusing the micelle/drug formulation into the body). The drug previously stabilized in the hydrophobic region of a micelle core will become insoluble due to the loss of micelle structures. This will severely reduce its

Author contributes:
Z.C., Y.L. and Z.Y designed the overall experiments. Y.L performed overall experiments. J.X and W.W. helped with TEM figures. E.Z and H.Z. helped with animal experiments. Z.C and Y.L outlined and wrote the paper. Z.C. supervised the study.

Data Availability. The authors declare that all data supporting the findings of this study are available within the paper and its supplementary information.

Additional Information:
Supplementary information is available for this paper. Correspondence and requests for materials should be addressed to Z.C.

Competing interests:
The authors declare no competing interests.

bioavailability and deteriorate its therapeutic performance.[3, 24, 25] This challenge remained insurmountable since all micelles have an apparent CMC, and can't keep stabilizing a hydrophobic cargo when diluted at the concentration below the CMC.[4]

Here we report that this stability challenge can be potentially solved by a so-called "sharp polarity contrast" micelle system (Fig. 1). In this sharp contrast system, each micelle molecule comprises a super hydrophilic zwitterionic polymer domain and a super hydrophobic lipid domain. The polarity contrast between the two domains is drastically "sharper" than most conventional micelle molecules. We found that sharp contrast micelle with an appropriate molecular weight (MW) of zwitterionic polymer has an undetectable ultra-low CMC below 2.7×10^{-6} mM. Such ultra-low CMC for micelles is exceedingly rare, and is at least six orders of magnitude lower than that for sodium dodecyl sulfate (SDS, CMC = 8.2 mM; commonly found in cleaning and hygiene products), and four orders of magnitude lower than Polysorbate 80 (CMC = 0.012 mM; widely used to formulate drugs, e.g., chemo drug docetaxel under the trade name of TAXOTERE®[26–28]). The mechanism of using zwitterionic moiety to increase micelle stability appears to be universal and very powerful. Even when a zwitterionic moiety or polymer was added into a micelle solution (not chemically modifying the micelle), the existing micelle molecules in the new solution was stabilized even at a concentration below its inherent CMC. We demonstrated that the ultra-low CMC micelle can remarkably stabilize hydrophobic cargoes (without micelle dissociation) in extremely diluted conditions, including clinically relevant dilution condition in serum while conventional micelles failed. To prove the promising use of ultra-low CMC micelles as next generation carriers, we prepared a simple docetaxel formulation stabilized by the ultra-low CMC micelle and intravenously injected it to the mice inoculated with melanoma tumor (B16F10). This formulation performed drastically better than TAXOTERE®, and was able to fully eradicate the tumor. It is worth-mentioned that a complete elimination of melanoma solely based on chemotherapy has rarely been reported[29–34]. We attributed the boosted antitumor performance of the old drug to the unprecedented stabilization ability by the ultra-low CMC micelles. We expect the ultra-low CMC micelle can be broadly applied to improve the delivery and outcome of other drugs of high therapeutic values.

Micelle-forming DSPE-PCB 5K.

Sharp-contrast micelle-forming molecule, DSPE-PCB 5K (a zwitterionic carboxy betaine polymer (PCB) of 5000 Dalton molecular weight (MW) conjugated to 1,2-distearoyl-sn-glycero-3-phosphoethanolamine (DSPE) lipid) was synthesized following our previous method,[35] and its structure is shown in Fig. 1 DSPE-PCB 5K powder is extremely water-soluble, and its resulting micelles were imaged by transmission electron microscopy (TEM) (Fig. 2a). The size of this micelle was measured by dynamic light scattering (DLS) (Fig. 2b), with a hydrodynamic diameter of 20±3.5 nm (mean ± SD, N=3) in phosphate buffered saline (PBS). The hydrophobic core domain of DSPE-PCB 5K micelle was detected using pyrene as reflected by the decrease in the intensity ratio of the first to the third highest energy bands (I_1/I_3) in the emission spectra of pyrene from 1.7 in water to 1.1 in micelle solution (Supplementary Fig. S1), following our previous method.[36] It should be noted that PCB such as 5K Dalton molecule weight is extremely water soluble without forming particles or

aggregates (hydrodynamic diameter =3.7±1.0 nm). Aggregation Number (N_{agg}) of DSPE-PCB 5K micelle in water was 44, which was calculated from the ratio of an apparent molecular mass of micelle, measured via static light scattering[37], and the M_W for a single DSPE-PCB 5K chain.

Conventional methods cannot determine an ultra-low CMC.

CMC for DSPE-PCB 5K was determined to be 1.3 $\times 10^{-3}$ mM using the pyrene probe method (Supplementary Fig. S2).[36] The pyrene method is one of the most sensitive and precise methods of CMC determination.[38–40] However, it does not have sufficient sensitivity to measure a CMC below 10^{-3} mM[41] because the final concentration for pyrene is maintained at 6 $\times 10^{-4}$ mM (in our previous protocol as well as others[36, 42]) to give good quality fluorescent spectra. A micelle concentration approaching or below 10^{-4} mM cannot significantly change the aggregation behavior of pyrene, and potential micelle formation cannot be detected (as reflected by pyrene spectrum change). As a consequence, 1.3 $\times 10^{-3}$ mM as measured by the pyrene method can be an upper CMC estimation for DSPE-PCB 5K. There are other fluorescent dyes such as 2-p-toluidinylnaphthalene-6-sulfonate (TNS) and 1-anilinonaphthalene-8-sulfonate (ANS),[43–45] or other ways to determine CMC including light and X-ray scattering,[46, 47] surface tension study,[48, 49] and isothermal titration calorimetry.[50, 51] None of them can precisely detect a CMC < 10^{-4} mM. Limited success in determining a CMC < 10^{-4} mM has been achieved by extrapolation of CMC values of structurally-similar molecules[52] and through filtration of radioactively labeled surfactants.[53] However, these approaches are not readily available.

Verification of new method to determine CMC.

To explore a potential CMC below 10^{-6} M, we developed a “diluting-concentrating” method. An initial stable colloid was prepared by reducing soluble Au^{3+} ions to insoluble Au nanoparticles (NPs) in the presence of micelles at a concentration far above their CMCs. A very small Au NP (<5 nm) was formed as a non-soluble probe, partitioned into the hydrophobic core of a micelle stabilized. Au probe size was estimated from maximum absorbance peak of Au NP,[54] and also from the size increase from empty micelle to probe-loaded micelle (measured by DLS). The micelle-protected Au NPs were subject to serial dilutions in water, and extremely diluted micelle concentration can be reached. Potential aggregation of Au NPs resulted in an increase in both the hydrodynamic size of the colloid and the maximum absorbance wavelength for Au NPs,[54] as measured by DLS and UV-spectrometer, respectively. Consider the samples may be too diluted for these measurements, they were concentrated using a rotary evaporator at 35 °C under reduced pressure and then re-measured for these parameters. Potential aggregation of hydrophobic Au NP cannot be reversed by this concentrating process and was detected from their corresponding concentrated samples (Supplementary Text1). Since cargo aggregation is attributed to the dissociation of protecting micelles, this method indirectly detects the CMC values. A series of common micelles commercially available with known CMCs labeled by the manufacturers were used to verify this method, including non-ionic micelles (polysorbate 80, DSPE-PEG 5K and 2K), cationic micelles (hexadecyltrimethylammonium bromide (CTAB)), anionic micelles (sodium dodecyl sulfate (SDS)), zwitterionic carboxy betaine and sulfobetaine micelles with varied hydrophobic chain lengths (dodecyl dimethylglycine

(CB12C), N-Tetradecyl-N-N-Dimethylglycine (CB14C), 3-(decyldimethylammonio) propane sulfonate (SB10C), 3-(N,N-Dimethylpalmitylammonio)propane sulfonate (SB16C)). Representative measuring curves are shown in Fig. 3. Measuring curves for all samples tested are shown in Supplementary Fig. S3. Without exception, CMC values for all micelles are right positioned, below which both the hydrodynamic size of the colloid and the maximum absorbance wavelength for Au NP start to increase significantly (Student's t test, $p<0.05$). Similar to common probes for CMC determination (e.g., pyrene, dye molecules, etc.), the presence of Au NPs in the hydrophobic micelle core does not seem to influence the dissociation behavior of micelles or an artifact signifying that the colloid system does not aggregate at < CMC would appear.

DSPE-PCB 5K has an undetectable ultra-low CMC.

Using the validated "diluting-concentrating" method, DSPE-PCB 5K micelle protected Au NP does not show any signs of cargo aggregation at concentration down to **2.7×10^{-6} mM** (Fig. 3; no significant signal increase based on student's t test). Its CMC is considered ultra-low and below our current detection limit of **2.7×10^{-6} mM**. The detection limit can be potentially lowered by one order of magnitude by further diluting the micelles, e.g., into a 10 L container, and then concentrating 1–1.5 L each time (using the currect 2 L evaporation flask); this approach is laborsome and has little room to significantly lower the CMC detection limit. In contrast, DSPE-PEG 5K micelles, widely used to construct nanomedicines, have an apparent CMC about 1×10^{-3} mM, consistent with literature values[41, 55, 56], and dissociate at concentrations, at least, three orders of magnitude higher than DSPE-PCB 5K. Compared with DSPE-PCB 5K having multiple zwitterionic carboxy betaines as the polar group, CB14C contains only one zwitterionic carboxy betaine and has significantly higher CMC at 3.4×10^{-2} mM. To confirm that DSPE-PCB 5K truly has an ultra-low CMC, we performed the following experiments: 1) Au NP colloid was formed in the presence of PCB 5K replacing DSPE-PCB 5K and was found unstable (aggregate). Note that DSPE-PCB 5K/Au colloid was stable at room temperature for weeks without precipitation. This excludes the possibility of PCB tightly interacting with Au NPs, preventing dissociation of DSPE-PCB 5K micelles (an artifact of lowered CMC). 2) Au NP probe was replaced by cross-linked polystyrene (PS) NP probe. Following the same "diluting-concentrating" method, where colloid aggregation was detected by DLS, CMC results were obtained similarly to Fig. 3a, regardless of the probe used (Supplementary Fig. S4). It should be noted that both Au and crosslinked PS NPs are non-dissolvable under extremely diluted conditions. This is the key to obtaining reliable CMC measuring results. Dissolvable salt NPs (e.g., $CaCO_3$) were not found to work as a probe since they are released from the micelle at a diluted concentration below their water solubility and aggregated when concentrated to the concentration above their water solubility (Supplementary Fig. S5). 3) DSPE-PCB 5K micelle at extremely low concentration (2.7×10^{-6} mM) has been further observed using TEM (Supplementary Fig S6).

Zwitterionic PCB and its amount are critical to achieving ultra-low CMC property.

To explore the unique role of zwitterionic PCB contributing to ultra-low CMC property, we incubated either free form of CB moiety or PCB 5K (with multiple CB) at high concentration with conventional micelles (i.e., SDS and Polysorbate 80), and found that

conventional micelles were significantly stabilized in both cases (Fig. 4a, b, and Supplementary Fig. S7a, b). It should be noted that similar stabilizing effect has been found in both inorganic and organic salt solutions.[57, 58] We attribute this effect to the super-hydrophilicity of CB and PCB (similar to salts), which increases the polarity of the aqueous phase,[35, 59] strengthens the hydrophobic-hydrophobic interaction, and drives the micelle assembly at a concentration far below the micelle's inherent CMC. The presence of ethylene glycol oligomer (OEG) or polymer (PEG), in contrast, increased the CMC for conventional micelles (Fig. 4a, b, and Supplementary Fig. S7a, b), which is consistent with the literature.[60] OEG and PEG are known for their hydrophobic nature and tend to decrease the polarity of the aqueous environment,[35, 59] behaving the opposite to super hydrophilic CB and PCB (Supplementary Text2). We further examined the micelle stabilizing effect of CB or PCB 5K at a series of concentrations, and found that a minimum of roughly 200 mg/ml CB and 40 mg/ml PCB 5K were required to prevent the dissociation of conventional micelles, e.g., SDS and Polysorbate 80 (Supplementary Fig. S7c, d, e, f). Thus, the presence of zwitterionic CB moiety as polar groups for DSPE-PCB 5K appears to be the key to the ultra-low CMC property.

We further found that an appropriate molecular weight (MW) of PCB (amount of CB moieties per polymer) is critical for DSPE-PCB to achieve the lowest possible CMC (Fig. 4c, d). PCB MW is expected to be as high as possible to ensure the CMC lowering effect. However, PCB MW shouldn't be too large since micelles with longer hydrophilic polymer chain typically have an increased CMC (e.g., shown by hydrophilic polyvinylpyrrolidone (PVP)-hydrophobic alkyl chain micelles[41]). It appears that DSPE-PCB 5K has so far, the balanced PCB MW and achieves the lowest possible CMC < $\mathbf{10^{-6}}$ **mM** (undetectable), comparing with DSPE-PCB 2K (CMC= 1.2 – 6 $\times 10^{-5}$ mM) and 10K (CMC= 0.9 – 1.8 $\times 10^{-5}$ mM), and other reported micelles containing zwitterionic polymer block.[61]

Ultra-stability of ultra-low-CMC Micelle when diluted in serum.

One major challenge with drug delivery is the dissociation of carrier entities (e.g., micelles) as they are infused into the blood stream since the drug carrier is typically diluted below its CMC. Blood serum comprises a large number of proteins (albumin) that decompose micelles and bind with this surfactants.[62] Compared with water, dilution in serum is even more challenging for assembled carrier systems. Here we tested the stability of ultra-low CMC and conventional micelles in fetal bovine serum (FBS) using the Au NP probe at 0.055 mM micelle concentration (Fig. 5). We found that DSPE-PCB 5K (ultra-low CMC) showed excellent stability over 72 h. Conventional Polysorbate 80 and DSPE-PEG 5K micelles were not stable; for DSPE-PEG 5K, it dissociated at this concentration even above its CMC. The diluted micelle concentration tested (10^{-2} mM) is chosen by considering the situation of a 60 kg adult patient having 4.5 L blood receiving 75 mg/m^2 TAXOTERE® to treat breast cancer.[63] The hypothetical maximum micelle concentration (i.e. Polysorbate 80) in the blood is calculated to be 5.5×10^{-2} mM, assuming all drug was injected simultaneously. The reality is TAXOTERE® has to mix with infusion saline and be slowly infused (typically complete in one hour).[64] As drugs gradually enter the blood, they are immediately diluted, with micelle concentration significantly lower than 10^{-2} mM. Our serum stability test at

10^{-2} mM indicates that ultra-low-CMC micelle is far more stable than conventional ones as drug carriers at clinic-relevant concentrations.

Drastically increased antitumor performance of docetaxel stabilized by ultra-low-CMC micelle.

To study the applicability of using ultra-low CMC micelles to deliver real drugs, we chose docetaxel and prepared docetaxel/ DSPE-PCB 5K formulation using a simple thin-film hydration method (see Experimental Section)[65–68]. Our controls include docetaxel/ Polysorbate 80 and docetaxel/DSPE-PEG 5K, similarly made through thin-film hydration method, and TAXOTERE® formulated based on literature[63, 64, 69]. The weight ratios of drug over surfactant for all formulations were kept at 4%, which is the drug loading level for TAXOTERE®[66, 68]. The hydrodynamic diameters for all tested samples were around 22 nm as determined by DLS. However, after diluting these samples in FBS to reach micelle concentration of 5.5 X10^{-2} mM (the hypothetical maximum micelle concentration in the blood), only docetaxel/ DSPE-PCB 5K can maintain its hydrodynamic size, while all other control formulations appeared to be un-stable over the tested time period (Fig. 6a). Drug release profiles were determined by placing the formulations into Slide-A-Lyzer MINI dialysis microtubes (3500Da MW cutoff) and dialyzed against PBS at 37°C with gentle stirring. Docetaxel remained inside the dialysis tubes at different time points was quantified using HPLC to calculate drug release. DSPE-PCB 5K showed the highest retention of docetaxel compared with other control micelles, with 50% drug released in 3.7 h (Supplementary Fig.S8). The drug release mechanism in our formulation is expected to be based on drug dissolution or drug leaching. This has been indicated by our control study showing the zwitterionic micelles can stabilize non-dissolvable Au NPs and crosslinked PS NPs (Fig.5, Supplementary Fig. S4) but not dissolvable $CaCO_3$ NPs (Supplementary Fig. S5) at diluted concentrations. We further checked the stability of different docetaxel formulations after lyophilization. Results indicated that after lyophilization docetaxel/DSPE-PCB 5K maintained its original hydrodynamic size, while all control micelle formulations significantly aggregated (Supplementary Fig. S9).

The maximum tolerated dose (MTD) of docetaxel/ DSPE-PCB 5K was determined using healthy C57BL/6 mice to be 55 mg docetaxel/kg bodyweight, significantly higher than control formulations docetaxel/DSPE-PEG 5K (40 mg/kg), docetaxel/Polysorbate 80 (40 mg/kg), and TAXOTERE® (25 mg/kg) (Supplementary Fig. S10). To examine the anti-tumor activity of different docetaxel/micelle formulations, C57BL/6 mice were inoculated with B16F10 cells at right flank and on day 8 after inoculation received intravenous injection of drug formulations. The dose for all drug/micelle formulations was kept the same at 10 mg docetaxel/ kg body weight for 5 injections every other day. It was found that docetaxel/ DSPE-PCB 5K showed significantly better anti-tumor activity compared with all other micellar docetaxel formulations, including TAXOTERE® (Fig. 6b). All tumors treated with this formulation were eliminated by 33 days after the first treatment without recurrence over 70-day observation period after tumor innoculation (Fig. 6c, d). None of the control formulations based on docetaxel could fully inhibit the melanoma tumor, and in fact other chemo drugs have rarely shown a complete elimination to melanoma[28, 30, 32, 70–74].

To further investigate the *in vivo* circulation profile of docetaxel/DSPE-PCB 5K, different docetaxel formulations were injected intravenously to healthy C57/BL6 mice. At different time points blood samples were collected and the concentration of docetaxel in plasma was measured via HPLC. It was found that docetaxel/DSPE-PCB 5K showed significantly longer blood circulation than all other micellar docetaxel formulations (Fig. 6e). The α and β half-life of docetaxel/DSPE-PCB 5K were calculated to be 0.6 hour and 5.9 hour, while for TAXOTERE® these values were 4 min and 36 min, respectively. For bio-distribution, healthy C57/BL6 mice were treated with intravenously injection of different docetaxel formulations after inoculation of B16F10 cells. Bio-distribution of docetaxel at different time points has been further studied. Significantly higher tumor accumulation of docetaxel/ DSPE-PCB 5K was observed at 24 hours post injection compared with control formulations (Fig. 6f). Such enhanced drug accumulation to tumor site has been observed at as early as 2 hours after administration (Fig. S11). We attributed the remarkable antitumor performance of docetaxel in our formulation to the unprecedented stabilization ability by the ultra-low CMC micelles.

In summary, the Ultra-low CMC micelle will be applicable as a novel agent carrier based on its ultra-stability in protecting cargo (without dissociation) at extremely diluted conditions, including serum dilution at clinically relevant settings where conventional micelle systems fail. It is reasonable to predict that by replacing conventional micelles with the ultra-low CMC micelle, therapeutic outcome of the drug delivered shall be significantly promoted. Our data fully support this claim and show that the docetaxel/ ultra-low CMC micelle formulation can completely eliminate the melanoma tumor on mice, while most known chemotherapy, including TAXOTERE® was unable to do so. We expect the ultra-low CMC micelle can be utilized to enhance the delivery and therapeutic effects of other drugs in general.

Methods

Materials

DSPE-PCB 2K, 5K, and 10K were synthesized and characterized following the previously established method.[35] The molecular weight of NHS-PCB was characterized via Waters Breeze 2 system gel permeation chromatography (GPC) with Waters 2414 reflex detector. The mobile phase was phosphate buffered saline (PBS) at a flow rate of 1mL/min. Polysorbate 80, SDS, CTAB, HAuCl4, $NaBH_4$, styrene, divinylbenzene, trifluoroethanol were obtained from Sigma-Aldrich. (St. Louis, USA). DSPE-PEG 5K was obtained from Laysan Bio, Inc. (Arab, USA). CB12C, CB14C, SB10C. SB16C were obtained from Anatrace Product. LLC (Maumee, USA). Docetaxel was obtained from LC Laboratories (Woburn, USA). B16F10 cells were obtained from ATCC.

Preparation of Au NPs encapsulated by DSPE-PCB 5K:

CMC for DSPE-PCB 5K was determined via established pyrene method.[36] During a typical “Diluting-concentrating” method for CMC determination, a probe (<5 nm) is first loaded into micelle core at high micelle concentration (> CMC). To load Au NP probe, micelles and $HAuCl_4$ are dissolved in 10 ml deionized water and vigorously stirred at room temperature,

followed by dropwise addition of 1 ml $NaBH_4$ aqueous solution (micelle: Au: $NaBH_4$ (molar ratio) is typically 1: 1: 6; take CTAB for example, its concentration is 0.01 M > its CMC 0.92 mM). The solution turns red, and the stirring is kept for another 5 min. To load cross-linked PS NP probe, micelles, photo-initiator 2959, styrene and divinyl benzene (molar ratio is typically 1: 10: 1.5: 1; take DSPE-PCB 5K for example, its concentration is 0.3 mM) are sonicated in deionized water to form nano-emulsion, followed by 20 min reaction under UV light. Micelles with either Au NP or PS NP loaded are further purified through 10K MWCO ultrafiltration to remove rough materials forming the probes, and 0.2 μm filter to remove unexpected large particles. The size of the probes can be determined by DLS (Zetasizer Nano-ZS, Malvern Instruments) by taking the size difference between empty micelles and loaded micelles. For Au NP probe, its size can be additionally measured by the maximum absorbance wavelength using a UV-VIS spectrometer (Thermo Scientific Multiscan Go). During the diluting-contributing procedure for CMC determination, the liquid sample was not further treated with filtration.

Aggregation Number (N_{agg}) of DSPE-PCB 5K micelle was calculated from the ratio of an apparent molecular mass of micelle which was measured via static light scattering (SLS) and M_w for a single DSPE-PCB 5K chain. Apparent molecular mass of DSPE-PCB 5K micelle was obtained by measuring a series of samples with different concentrations (ranged from 1.2 g/L to 4.8 mg/L) via Malvern Zetasizer Nano-ZS.

Preparation of docetaxel/DSPE-PCB 5K formulation

To prepare docetaxel/DSPE-PCB 5K formulation, 150 mg of DSPE-PCB 5K and 6 mg docetaxel were co-dissolved in 5 ml trifluoroethanol in a round-bottom flask. The solvent was subsequently evaporated by rotary evaporation to obtain a thin film. The film was then kept in a vacuum for 2 hours at room temperature to remove the residual trifluoroethanol. After the addition of 3 ml saline and stirring at 800 rpm for 30 min, a clear micelle solution with docetaxel loaded was obtained. Docetaxel/DSPE-PEG 5K and docetaxel/Polysorbate 80 formulations were prepared following the same procedure. Taxotere was prepared follow the reference[63, 64, 69]. The weight ratios of drug over surfactant for all formulations were kept at 4%, which is the drug loading level for TAXOTERE®[66, 68].

Drug release profiles were determined by placing 100 μL different formulations into Slide-A-Lyzer MINI dialysis microtubes (3500 Da MW cutoff) and dialyzed against PBS at 37°C with gentle stirring. At different time intervals, docetaxel remained in the dialyzer was quantified through HPLC by a Waters Breeze 2 System equipped with a Waters 2998 photodiode array detector at 230 nm and a Waters symmetry C_{18} column (4.6×7.5 mm). The mobile phase was a mixture of acetonitrile/water (50%:50% volume) at a flow rate of 1 mL/min. The docetaxel showed a single elution peak at 5.47 min.

Animal experiments

Animal experiment was approved by the Institutional Animal Care and Use Committee (IACUC) of Wayne State University, and performed in compliance with the relevant laws and institutional guidelines. B16F10 cells (ATCC, CRL-6475) were culture in RPMI 1640 medium containing 10% fetal bovine serum at 37 °C under 5% CO_2 atmosphere. For *in vivo*

tumor therapeutic study, healthy C57BL/6 mice (7 weeks old, 20–25 g) received a subcutaneous injection of 100 μL B16F10 cells (5×10^6 cells/mL) at the right flank. After 8 days of inoculation, the tumor became visible, and different formulations were administered by intravenous injection via tail vein 5 times every other day at the dosage of 10 mg docetaxel/kg body weight. The tumor volume of the mice was measured day by day and calculated with an equation of $(L\times W^2)/2$ where L is the long length and W is the short length of the tumor. Mice were euthanized if their weight loss exceeded 15% or if their tumor grew to a volume greater than 1000 mm^3. For MTD study, healthy C57BL/6 mice received one intravenous injection of different docetaxel formulations through the tail vein at the dose of 25 mg/kg, 40 mg/kg, and 55 mg/kg. Treated mice were subsequently observed day by day and checked for mortality, body weight and signs of toxicity. To test docetaxel concentration in plasma, healthy C57BL/6 mice (7 weeks old, 20–25g) were treated with intravenous injection via tail vein at the dosage of 10 mg/kg. At different time intervals, 50 μL blood samples were collected and transferred to sodium heparin treated tubes. Docetaxel was extracted from the plasma supernatant by ethyl acetate and the extracted solution was evaporated under a gentle stream of nitrogen. The extraction residues were reconstituted in the mixture of acetonitrile/water (50%:50% volume). The docetaxel concentration was measured using HPLC as mentioned above.

To test bio-distribution, healthy C57BL/6 mice (7 weeks old, 20–25g) received a subcutaneous injection of 100 μL B16F10 cells (5×10^6 cells/mL) at the right flank. After 8 days of inoculation when tumors became visible, different formulations were administered by intravenous injection via tail vein. Mice were euthanized at certain time point. Organs such as liver, heart, kidney, spleen, lung and tumor tissues were collected, thoroughly washed with saline (0.9% NaCl), weighted and stored for further analysis. Organs or tissues were homogenized with Mini-beadbeater-24 (Biospec Products, Inc., USA) in acetonitrile/water (50%:50% volume). The resulting 200 μL samples of homogenized tissue were mixed with 1 mL ethyl acetate. The samples were extracted on a vortex mixer for 2 minutes then centrifuged at 4000 g for 5 minutes. The organic layer was transferred to a clean tube and evaporated under a gentle stream of nitrogen. The extraction residue was reconstituted in 1 mL mixture of acetonitrile/water (50%:50% volume). The docetaxel concentration was measured using HPLC.

Statistical Analysis

n = 7 was used for mice per treatment group unless specified otherwise. The sample size was selected according to previous reports. All tested mice were included in analyses except for ones with unforeseen sickness or morbidity. Animal cohorts where randomly selected and investigator were not blind to performed experiments. Most data were normally distributed and similar variance was determined for groups that are compared. Analysis includes unpaired two-tailed t-test and one-way analysis of variance (ANOVA) with Bonferroni multiple-comparison correction. For data not following normal distribution, non-parametric Mann-Whitney test was used. *: $P < 0.01$, **: $P < 0.001$, ***: $P < 0.0001$ and n.s.: no significant difference. For all statistical analysis, significance was accepted at the 95% confidence level, and all analyses were two-tailed.

Supplementary Material

Refer to Web version on PubMed Central for supplementary material.

Acknowledgements

This work was supported by the faculty start-up fund at Wayne State University, the National Science Foundation (DMR-1410853), and the National Institute of Diabetes and Digestive and Kidney Diseases of the National Institutes of Health (DP2DK111910). This work made use of the JEOL 2010 TEM supported by National Science Foundation Award, 0216084. We thank Cheng-Hua Liu and Dr. Wei Zhang at Michigan State University for their support on static light scattering measurements.

Reference

1. O'Reilly RK, Hawker CJ & Wooley KL Cross-linked block copolymer micelles: functional nanostructures of great potential and versatility. Chemical Society Reviews 35, 1068–1083 (2006). [PubMed: 17057836]
2. Rodriguez-Hernandez J, Checot F, Gnanou Y & Lecommandoux S Toward 'smart' nano-objects by self-assembly of block copolymers in solution. Progress in Polymer Science 30, 691–724 (2005).
3. Kim S, Shi YZ, Kim JY, Park K & Cheng JX Overcoming the barriers in micellar drug delivery: loading efficiency, in vivo stability, and micelle-cell interaction. Expert Opinion on Drug Delivery 7, 49–62 (2010). [PubMed: 20017660]
4. Ahmad Z, Shah A, Siddiq M & Kraatz HB Polymeric micelles as drug delivery vehicles. Rsc Adv 4, 17028–17038 (2014).
5. Verma G & Hassan PA Self assembled materials: design strategies and drug delivery perspectives. Physical Chemistry Chemical Physics 15, 17016–17028 (2013). [PubMed: 23907560]
6. Kamaly N, Xiao ZY, Valencia PM, Radovic-Moreno AF & Farokhzad OC Targeted polymeric therapeutic nanoparticles: design, development and clinical translation. Chemical Society Reviews 41, 2971–3010 (2012). [PubMed: 22388185]
7. Service RF NANOTECHNOLOGY Nanoparticle Trojan Horses Gallop From the Lab Into the Clinic. Science 330, 314–315 (2010). [PubMed: 20947742]
8. Zhang L et al. Nanoparticles in medicine: Therapeutic applications and developments. Clinical Pharmacology & Therapeutics 83, 761–769 (2008). [PubMed: 17957183]
9. Service RF Nanotechnology takes aim at cancer. Science 310, 1132–1134 (2005). [PubMed: 16293748]
10. Yoo JW, Irvine DJ, Discher DE & Mitragotri S Bio-inspired, bioengineered and biomimetic drug delivery carriers. Nat Rev Drug Discov 10, 521–535 (2011). [PubMed: 21720407]
11. Scheinberg DA, Villa CH, Escorcia FE & McDevitt MR Conscripts of the infinite armada: systemic cancer therapy using nanomaterials. Nat Rev Clin Oncol 7, 266–276 (2010). [PubMed: 20351700]
12. Petros RA & DeSimone JM Strategies in the design of nanoparticles for therapeutic applications. Nat Rev Drug Discov 9, 615–627 (2010). [PubMed: 20616808]
13. Kim S, Kim JH, Jeon O, Kwon IC & Park K Engineered Polymers for Advanced Drug Delivery. Eur. J. Pharm. Biopharm 71, 420–430 (2009). [PubMed: 18977434]
14. Guo S & Huang L Nanoparticles containing insoluble drug for cancer therapy. Biotechnology Advances 32, 778–788 (2014). [PubMed: 24113214]
15. Guo S, Miao L, Wang Y & Huang L Unmodified drug used as a material to construct nanoparticles: delivery of cisplatin for enhanced anti-cancer therapy. Journal of Controlled Release 174, 137–142 (2014). [PubMed: 24280262]
16. Tang L et al. Investigating the optimal size of anticancer nanomedicine. Proceedings of the National Academy of Sciences of the United States of America 111, 15344–15349 (2014). [PubMed: 25316794]
17. Tong R et al. Smart Chemistry in Polymeric Nanomedicines. Chemical Society Reviews 43, 6982–7012 (2014). [PubMed: 24948004]

18. Hu CMJ et al. Erythrocyte membrane-camouflaged polymeric nanoparticles as a biomimetic delivery platform. Proceedings of the National Academy of Sciences of the United States of America 108, 10980–10985 (2011). [PubMed: 21690347]
19. Judd J et al. Tunable Protease-Activatable Virus Nanonodes. ACS Nano 8, 4740–4746 (2014). [PubMed: 24796495]
20. Lee J et al. Caveolae-Mediated Endocytosis of Conjugated Polymer Nanoparticles. Macromolecular Bioscience 13, 913–920 (2013). [PubMed: 23629923]
21. Wang M, Alberti KA, Sun S & Xu Q Efficient Intracellular Protein Delivery for Cancer Therapy using Combinatorial Lipid-like Nanoparticles. Angewandte Chemie-International Edition 53, 2893–2898 (2014). [PubMed: 24519972]
22. Shukla S & Steinmetz NF Virus-based nanomaterials as positron emission tomography and magnetic resonance contrast agents: from technology development to translational medicine. WIREs Nanomedicine and Nanobiotechnology **DOI:** 10.1002/wnan.1335 (2015).**DOI:**
23. Rosler A, Vandermeulen GWM & Klok HA Advanced drug delivery devices via self-assembly of amphiphilic block copolymers. Advanced Drug Delivery Reviews 53, 95–108 (2001). [PubMed: 11733119]
24. Feng L & Mumper RJ A critical review of lipid-based nanoparticles for taxane delivery. Cancer Lett 334, 157–175 (2013). [PubMed: 22796606]
25. Chen H et al. Release of hydrophobic molecules from polymer micelles into cell membranes revealed by Forster resonance energy transfer imaging. Proceedings of the National Academy of Sciences of the United States of America 105, 6596–6601 (2008). [PubMed: 18445654]
26. Montero A, Fossella F, Hortobagyi G & Valero V Docetaxel for treatment of solid tumours: a systematic review of clinical data. Lancet Oncol 6, 229–239 (2005). [PubMed: 15811618]
27. Vanoosterom AT & Schriivers D Docetaxel (Taxotere(R)), a Review of Preclinical and Clinical-Experience .2. Clinical-Experience. Anti-Cancer Drug 6, 356–368 (1995).
28. Bissery MC, Nohynek G, Sanderink GJ & Lavelle F Docetaxel (Taxotere): a review of preclinical and clinical experience. Part I: Preclinical experience. Anticancer Drugs 6, 339–355, 363–338 (1995). [PubMed: 7670132]
29. Sadhu SS et al. In Vitro and In Vivo Tumor Growth Inhibition by Glutathione Disulfide Liposomes. Cancer Growth and Metastasis 10, 1179064417696070 (2017).
30. Cruz-Munoz W, Man S & Kerbel RS Effective Treatment of Advanced Human Melanoma Metastasis in Immunodeficient Mice Using Combination Metronomic Chemotherapy Regimens. Clinical Cancer Research 15, 4867–4874 (2009). [PubMed: 19622578]
31. Feleszko W, Zagożdżon R, Gołb J & Jakóbisiak M Potentiated antitumour effects of cisplatin and lovastatin against MmB16 melanoma in mice. European Journal of Cancer 34, 406–411 (1998). [PubMed: 9640231]
32. Gao C et al. Jolkinolide B induces apoptosis and inhibits tumor growth in mouse melanoma B16F10 cells by altering glycolysis. Scientific Reports 6, 36114 (2016). [PubMed: 27796318]
33. Jin J. l. et al. PTD4-apoptin protein and dacarbazine show a synergistic antitumor effect on B16-F1 melanoma in vitro and in vivo. European Journal of Pharmacology 654, 17–25 (2011). [PubMed: 21184754]
34. Lee C et al. Fasting Cycles Retard Growth of Tumors and Sensitize a Range of Cancer Cell Types to Chemotherapy. Science Translational Medicine 4, 124ra127–124ra127 (2012).
35. Cao ZQ, Zhang L & Jiang SY Superhydrophilic Zwitterionic Polymers Stabilize Liposomes. Langmuir 28, 11625–11632 (2012). [PubMed: 22783927]
36. Cao ZQ et al. Toward an understanding of thermoresponsive transition behavior of hydrophobically modified N-isopropylacrylamide copolymer solution. Polymer 46, 5268–5277 (2005).
37. Imae T & Ikeda S Sphere-rod transition of micelles of tetradecyltrimethylammonium halides in aqueous sodium halide solutions and flexibility and entanglement of long rodlike micelles. The Journal of Physical Chemistry 90, 5216–5223 (1986).
38. Ananthapadmanabhan KP, Goddard ED, Turro NJ & Kuo PL Fluorescence Probes for Critical Micelle Concentration. Langmuir 1, 352–355 (1985). [PubMed: 21370917]

39. La SB, Okano T & Kataoka K Preparation and characterization of the micelle-forming polymeric drug indomethacin-incorporated poly(ethylene oxide)-poly(beta-benzyl L-aspartate) block copolymer micelles. Journal of Pharmaceutical Sciences 85, 85–90 (1996). [PubMed: 8926590]
40. Allen C, Yu Y, Maysinger D & Eisenberg A Polycaprolactone-b-poly(ethylene oxide) block copolymer micelles as a novel drug delivery vehicle for neurotrophic agents FK506 and L-685,818. Bioconjug Chem 9, 564–572 (1998). [PubMed: 9736490]
41. Lukyanov AN & Torchilin VP Micelles from lipid derivatives of water-soluble polymers as delivery systems for poorly soluble drugs. Adv Drug Deliver Rev 56, 1273–1289 (2004).
42. Lee JH et al. Polymeric nanoparticle composed of fatty acids and poly(ethylene glycol) as a drug carrier. Int J Pharmaceut 251, 23–32 (2003).
43. Nakagaki M, Komatsu H & Handa T Estimation of Critical Micelle Concentrations of Lysolecithins with Fluorescent-Probes. Chem Pharm Bull 34, 4479–4485 (1986).
44. Matsuzaki K et al. Quantitative-Analysis of Hemolytic Action of Lysophosphatidylcholines Invitro - Effect of Acyl Chain Structure. Chem Pharm Bull 36, 4253–4260 (1988). [PubMed: 3246000]
45. Katsu T Reinvestigation of the Critical Micelle Concentrations of Cationic Surfactants with the Use of an Ammonium 8-Anilino-1-Naphthalenesulphonate Fluorescent-Probe. Colloid Surface 60, 199–202 (1991).
46. Hadjichristidis N, Pispas S & Floudas GA Block copolymers: synthetic strategies, physical properties, and applications. (Wiley, New York; 2003).
47. Topel O, Cakir BA, Budama L & Hoda N Determination of critical micelle concentration of polybutadiene-block-poly(ethyleneoxide) diblock copolymer by fluorescence spectroscopy and dynamic light scattering. J Mol Liq 177, 40–43 (2013).
48. Carnero Ruiz C et al. Effect of ethylene glycol on the thermodynamic and micellar properties of Tween 20. Colloid and Polymer Science 281, 531–541 (2003).
49. Kramp W, Pieroni G, Pinckard RN & Hanahan DJ Observations on the Critical Micellar Concentration of 1-O-Alkyl-2-Acetyl-Sn-Glycero-3-Phosphocholine and a Series of Its Homologs and Analogs. Chem Phys Lipids 35, 49–62 (1984). [PubMed: 6744496]
50. Henriksen JR, Andresen TL, Feldborg LN, Duelund L & Ipsen JH Understanding Detergent Effects on Lipid Membranes: A Model Study of Lysolipids. Biophys J 98, 2199–2205 (2010). [PubMed: 20483328]
51. Hoyrup P, Davidsen J & Jorgensen K Lipid membrane partitioning of lysolipids and fatty acids: Effects of membrane phase structure and detergent chain length. J Phys Chem B 105, 2649–2657 (2001).
52. Weltzien HU Cytolytic and Membrane-Perturbing Properties of Lysophosphatidylcholine. Biochimica Et Biophysica Acta 559, 259–287 (1979). [PubMed: 476122]
53. Smith R & Tanford C Critical Micelle Concentration of L-Alpha-Dipalmitoylphosphatidylcholine in Water and Water/Methanol Solutions. Journal of Molecular Biology 67, 75–83 (1972). [PubMed: 5042465]
54. Berges DA et al. Studies on the active site of succinyl-CoA:tetrahydrodipicolinate N-succinyltransferase. Characterization using analogs of tetrahydrodipicolinate. The Journal of biological chemistry 261, 6160–6167 (1986). [PubMed: 3700390]
55. Ashok B, Arleth L, Hjelm RP, Rubinstein I & Onyuksel H In vitro characterization of PEGylated phospholipid micelles for improved drug solubilization: effects of PEG chain length and PC incorporation. J Pharm Sci 93, 2476–2487 (2004). [PubMed: 15349957]
56. Uster PS et al. Insertion of poly(ethylene glycol) derivatized phospholipid into pre-formed liposomes results in prolonged in vivo circulation time. FEBS Letters 386, 243–246 (1996). [PubMed: 8647291]
57. Yu DF et al. Effects of Inorganic and Organic Salts on Aggregation Behavior of Cationic Gemini Surfactants. J Phys Chem B 114, 14955–14964 (2010). [PubMed: 21028805]
58. Miyagishi S, Okada K & Asakawa T Salt effect on critical micelle concentrations of nonionic surfactants, N-acyl-N-methylglucamides (MEGA-n). Journal of Colloid and Interface Science 238, 91–95 (2001). [PubMed: 11350141]
59. Cao ZQ & Jiang SY Super-hydrophilic zwitterionic poly(carboxybetaine) and amphiphilic non-ionic poly(ethylene glycol) for stealth nanoparticles. Nano Today 7, 404–413 (2012).

60. Ruiz CC et al. Effect of ethylene glycol on the thermodynamic and micellar properties of Tween 20. Colloid and Polymer Science 281, 531–541 (2003).
61. Yusa S. i., Fukuda K, Yamamoto T, Ishihara K & Morishima Y Synthesis of well-defined amphiphilic block copolymers having phospholipid polymer sequences as a novel biocompatible polymer micelle reagent. Biomacromolecules 6, 663–670 (2005). [PubMed: 15762627]
62. Liu H et al. Structure-based programming of lymph-node targeting in molecular vaccines. Nature 507, 519–522 (2014). [PubMed: 24531764]
63. Anderson JM, Rodriguez A & Chang DT Foreign body reaction to biomaterials. Semin Immunol 20, 86–100 (2008). [PubMed: 18162407]
64. Hart M & Acott S Physical and chemical stability of Taxotere® (docetaxel) one-vial (20 mg/ml) infusion solution following refrigerated storage. Ecancermedicalscience 4, 202 (2010). [PubMed: 22276044]
65. Le Garrec D et al. Preparation, characterization, cytotoxicity and biodistribution of docetaxel-loaded polymeric micelle formulations. Journal of Drug Delivery Science and Technology 15, 115–120 (2005).
66. Jun YJ et al. Stable and efficient delivery of docetaxel by micelle-encapsulation using a tripodal cyclotriphosphazene amphiphile. Int J Pharmaceut 422, 374–380 (2012).
67. Chen L et al. Pluronic P105/F127 mixed micelles for the delivery of docetaxel against Taxol-resistant non-small cell lung cancer: optimization and in vitro, in vivo evaluation. Int J Nanomedicine 8, 73–84 (2013). [PubMed: 23319859]
68. Wang Y et al. PEG–PCL based micelle hydrogels as oral docetaxel delivery systems for breast cancer therapy. Biomaterials 35, 6972–6985 (2014). [PubMed: 24836952]
69. Bissery MC, Nohynek G, Sanderink GJ & Lavelle F Docetaxel (Taxotere(R)) - a Review of Preclinical and Clinical-Experience .1. Preclinical Experience. Anti-Cancer Drug 6, 339–355 (1995).
70. Sadhu SS et al. In Vitro and In Vivo Tumor Growth Inhibition by Glutathione Disulfide Liposomes. Cancer Growth and Metastasis 10, 0–0 (2017).
71. Wack C, Becker JC, Brocker EB, Lutz WK & Fischer WH Chemoimmunotherapy for melanoma with dacarbazine and 2,4-dinitrochlorobenzene: results from a murine tumour model. Melanoma research 11, 247–253 (2001). [PubMed: 11468513]
72. Kerr DE et al. Regressions and cures of melanoma xenografts following treatment with monoclonal antibody β-lactamase conjugates in combination with anticancer prodrugs. Cancer research 55, 3558–3563 (1995). [PubMed: 7627964]
73. Luke JJ & Schwartz GK Chemotherapy in the management of advanced cutaneous malignant melanoma. Clinics in Dermatology 31, 290–297 (2013). [PubMed: 23608448]
74. Saito R.d.F., Tortelli TC Jr, Jacomassi MDA, Otake AH & Chammas R Emerging targets for combination therapy in melanomas. FEBS Letters 589, 3438–3448 (2015). [PubMed: 26450371]

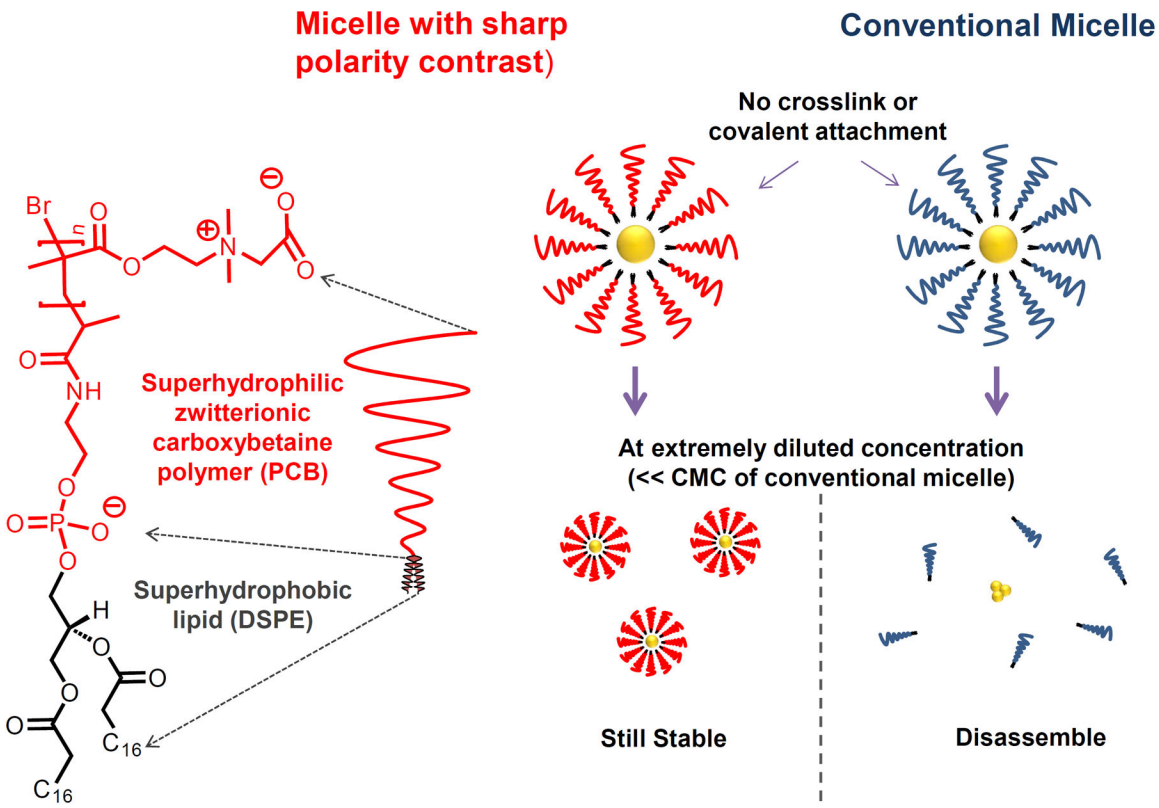

Figure 1|. Ultra-low-CMC micelles and their unusual ability to stabilize cargoes in extremely diluted conditions with micelle concentrations far below CMCs of common micelles.

Conventional micelles dissociate at a concentration below CMC, and thus can't stabilize a hydrophobic cargo. Molecular structure for ultra-low-CMC micelle is shown. For conventional micelles, their polar groups were either non-ionic (e.g., polysorbate 80, having hydrophobic nature), or only contained one ionic group (e.g., sodium dodecyl sulfate). Sharp contrast micelle with multiple polar zwitterionic (polyzwitterionic) groups was recently reported[35].

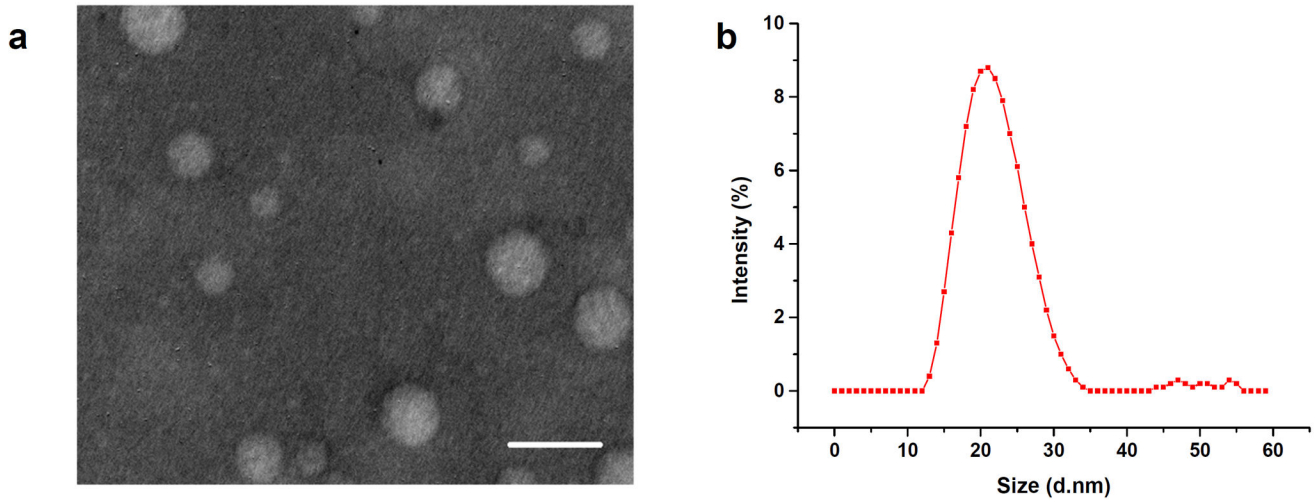

Figure 2 |. TEM and DLS data of DSPE-PCB 5K micelle.

a, Representative TEM image for DSPE-PCB 5K micelle (5 mM) in water taken by JEOL 2010 Transmission electron microscopy. Stained with 2% uranyl acetate. The scale bar in the figure is 50 nm. **b,** DLS data for DSPE-PCB 5K in PBS (0.5mM), showing an average diameter of 20 ± 3.5 nm (mean ± SD, N = 3) with PDI of 0.13.

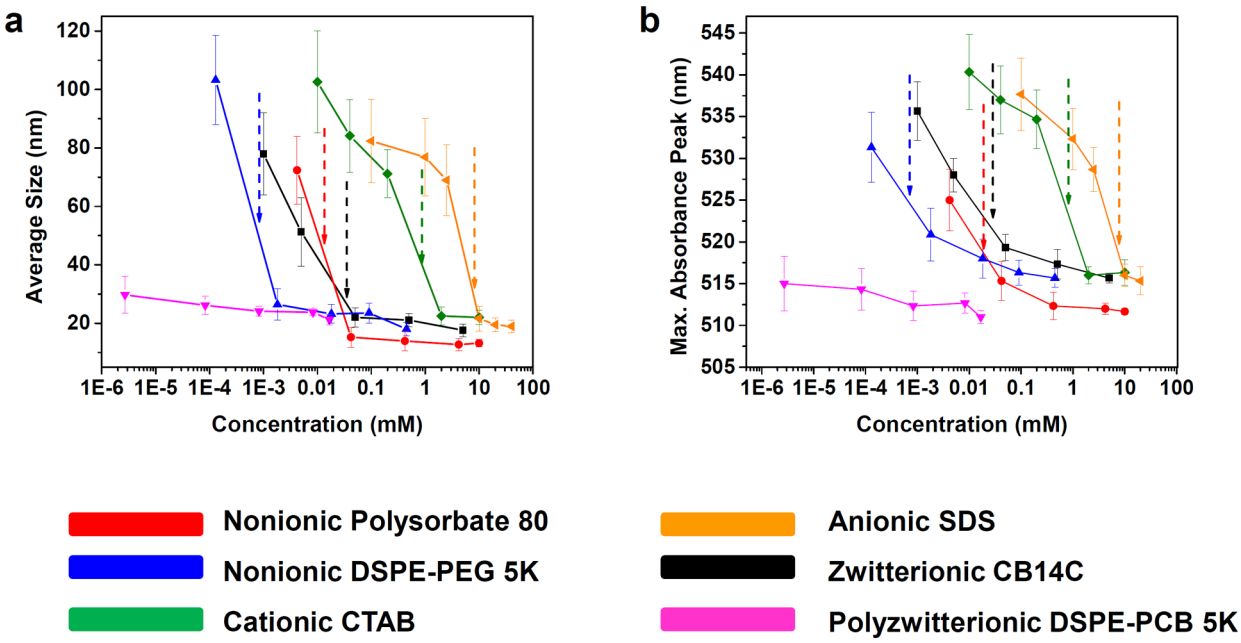

Figure 3 |. "Diluting-concentrating" method to probe CMCs for micelles.

Aggregation of Au probe at different micelle concentrations was reflected by **a,** hydrodynamic size of the colloid and **b,** Au maximum absorbance wavelength (mean ± SD, N=3). Known CMC values for micelles were indicated by dotted arrows. CMC data for DSPE-PEG are from reference.[41, 55, 56]

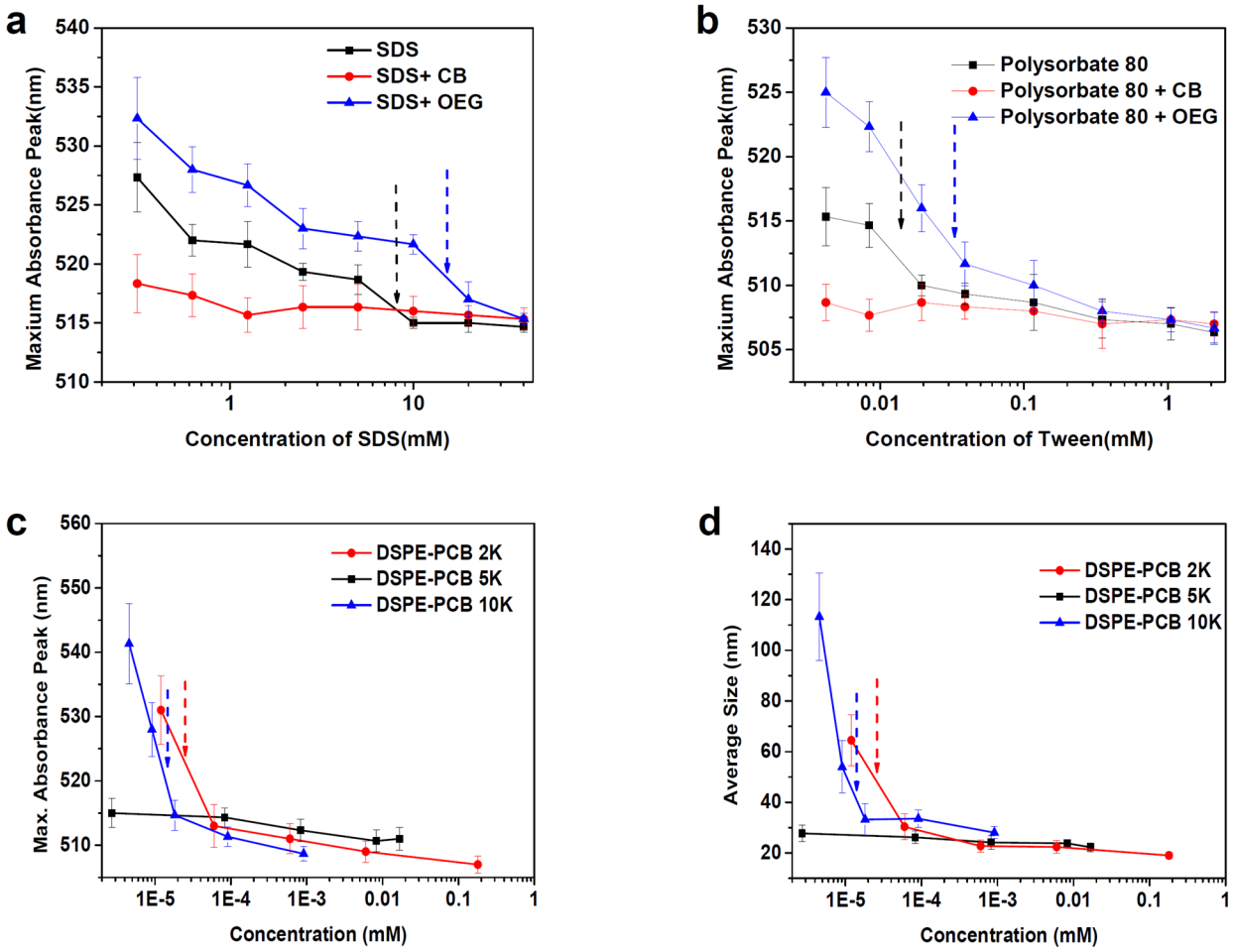

Figure 4 |. Supplying zwitterionic moieties decreases CMCs of conventional micelles, and the impact of zwitterionic PCB MW on the CMC of DSPE-PCB.

Au NPs were loaded in a, SDS and b, Polysorbate 80, respectively, and upon water dilution, their aggregation behavior (due to micelle dissociation) was measured by the increase in maximum absorbance peak of Au (mean ± SD, N=3). When 500 mg/ml carboxy betaine (CB) was used as dilution solvent, no significant Au aggregation was observed in the dilution range, indicating a significantly stabilized micelle in such environment, even at a concentration below its inherent CMC. In contrast, when 500 mg/ml OEG was used as dilution solvent, there was Au NP aggregation at high micelle concentrations, showing an increase of micelle CMC. CB and OEG alone (without the aid of micelles) can't stabilize Au NPs, leading to severe aggregation. It should be noted that DLS data are not reliable in this experiment since the large concentration of small size CB or OEG interferes with the hydrodynamic size readings for aggregated Au NPs. **c, d,** "Diluting-concentrating" method to probe CMCs for DSPE-PCB 2K, 5K, 10K micelles. Aggregation of Au probe at different micelle concentrations was reflected by c, hydrodynamic size of the colloid (mean ± SD, N=3) and d), Au maximum absorbance wavelength (mean ± SD, N=3). CMC values determined for DSPE-PCB 2K and 10K were indicated by dotted arrows.

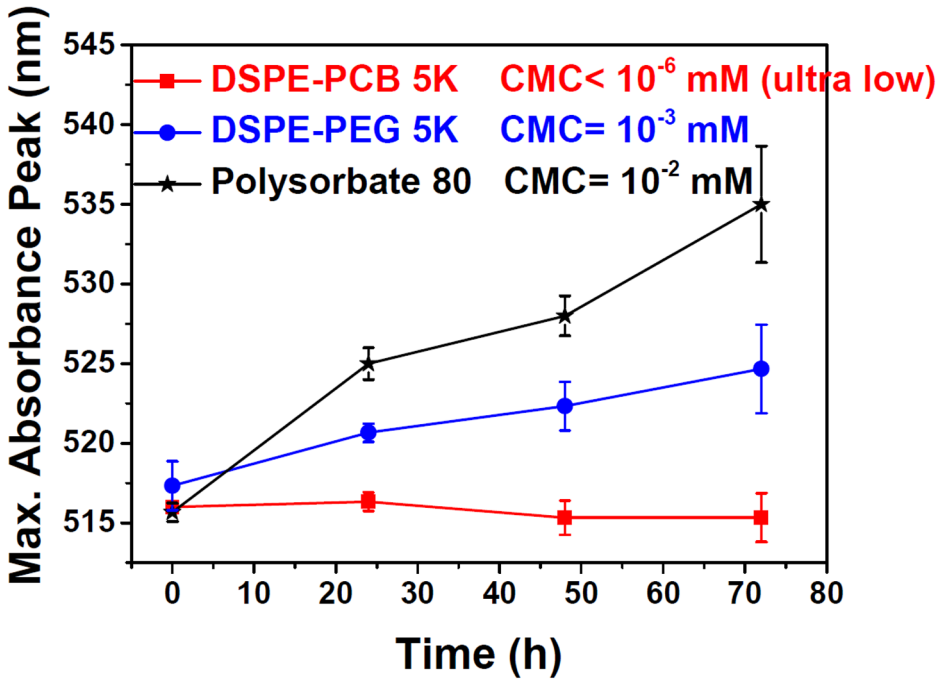

Figure 5 |. Stability of ultra-low-CMC micelle and conventional micelles with Au NP probe encapsulated at 5.5 X10^{-2} mM micelle concentration in 100% fetal bovine serum (FBS) over 72 h at room temperature.

Potential micelle disassociation resulted in Au NP aggregation, which was measured by Au maximum absorbance peak (mean ± SD, N=3). Known CMC values for each micelle are indicated inside the graph.

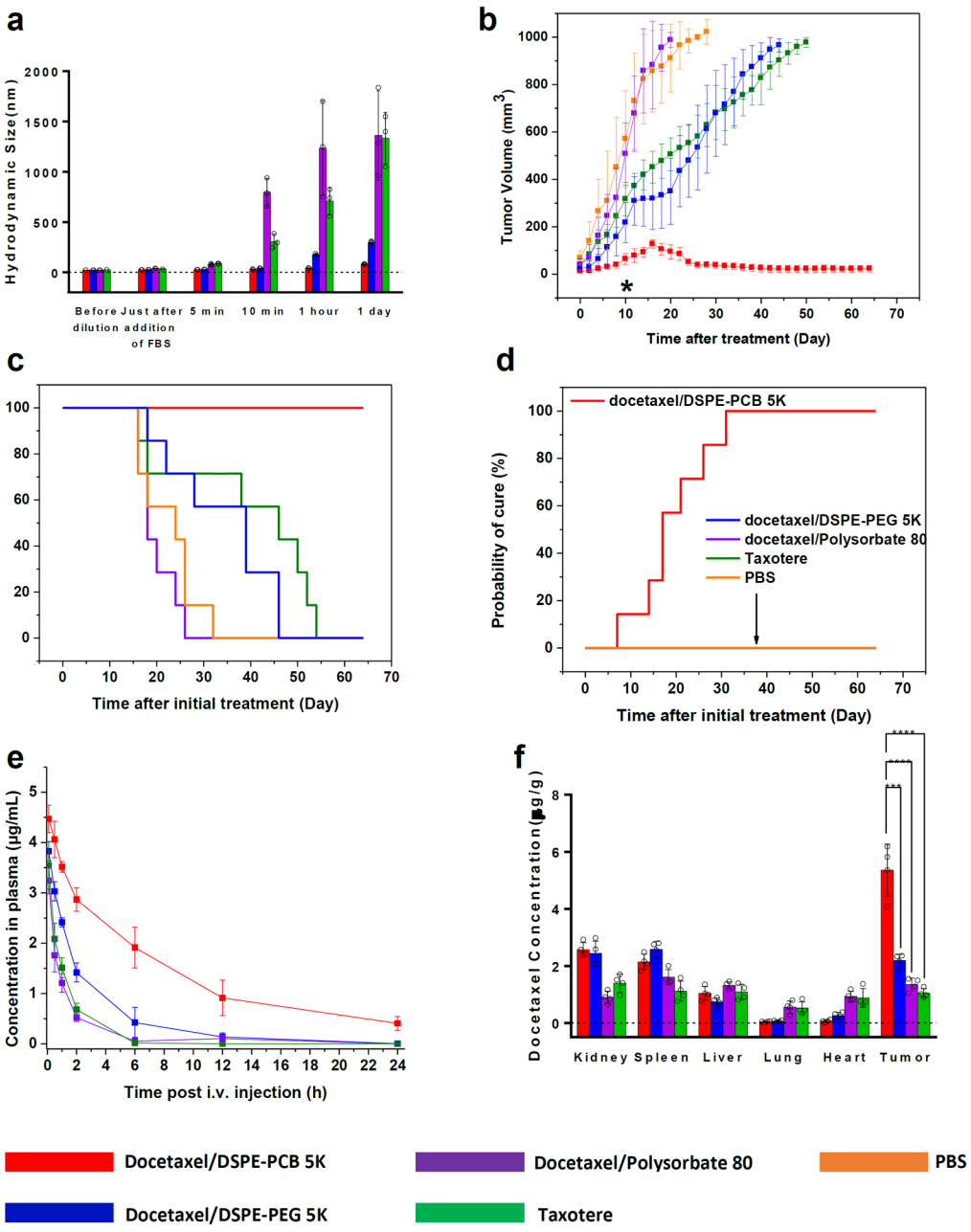

Figure 6 |. Stability of docetaxel/DSPE-PCB 5K formulation and its anti-tumor performance compared with other control formulations.

a, stability of different docetaxel formulation diluted in FBS (mean ± SD, N=3). **b,** Anti-tumor performance of docetaxel/DSPE-PCB 5K formulation (mean ± SD, N = 7) compared with other formulations (mean ± SD, N = 7). On day 10 after treatment (*), a Mann-Whitney Test indicated that docetaxel/DSPE-PCB 5K delayed the tumor growth greater than all other four controls at $p = 0.005$. **c,** Survival rate curve of mice treated with different formulation. **d,** Probability of cure. In mice bearing invisible tumors < 1 mm^3 in size or mice in which flattened and darkened scar tissue developed, it was considered that the tumor had been completely eradicated. **e**, concentration of docetaxel in blood plasma of different

formulations (mean ± SD, N = 4). **f**, bio-distribution of different docetaxel formulations 24 hours post i.v. injection (mean ± SD, N= 4). One-Way ANOVA analysis with Bonferroni multi-comparison: significant difference between docetaxel/DSPE-PCB 5K and docetaxel/DSPE-PEG 5K, docetaxel/DSPE-PCB 5K and docetaxel/Polysorbate 80, docetaxel/DSPE-PCB 5K and Taxotere, at $p < 0.001$ (***), $p < 0.0001$ (****), and $p < 0.0001$ (****), respectively.